A Quantitative Systems Pharmacology Platform to Investigate the Impact of Alirocumab and Cholesterol-Lowering Therapies on Lipid Profiles and Plaque Characteristics

Gene Regulation and Systems Biology
Volume 11: 1–15

DOI: 10.1177/1177625017710941

Jeffrey E Ming[1], Ruth E Abrams[1], Derek W Bartlett[2], Mengdi Tao[1], Tu Nguyen[1], Howard Surks[1], Katherine Kudrycki[2], Ananth Kadambi[2], Christina M Friedrich[2], Nassim Djebli[1], Britta Goebel[1], Alex Koszycki[1], Meera Varshnaya[1], Joseph Elassal[3], Poulabi Banerjee[3], William J Sasiela[3], Michael J Reed[2], Jeffrey S Barrett[1] and Karim Azer[1]

[1]Sanofi, Bridgewater, NJ, USA; Frankfurt Am Main, Germany, and Montpellier, France.
[2]Rosa & Co, San Carlos, CA, USA. [3]Regeneron, Tarrytown, NY, USA.

ABSTRACT: Reduction in low-density lipoprotein cholesterol (LDL-C) is associated with decreased risk for cardiovascular disease. Alirocumab, an antibody to proprotein convertase subtilisin/kexin type 9 (PCSK9), significantly reduces LDL-C. Here, we report development of a quantitative systems pharmacology (QSP) model integrating peripheral and liver cholesterol metabolism, as well as PCSK9 function, to examine the mechanisms of action of alirocumab and other lipid-lowering therapies, including statins. The model predicts changes in LDL-C and other lipids that are consistent with effects observed in clinical trials of single or combined treatments of alirocumab and other treatments. An exploratory model to examine the effects of lipid levels on plaque dynamics was also developed. The QSP platform, on further development and qualification, may support dose optimization and clinical trial design for PCSK9 inhibitors and lipid-modulating drugs. It may also improve our understanding of factors affecting therapeutic responses in different phenotypes of dyslipidemia and cardiovascular disease.

KEYWORDS: Quantitative systems pharmacology model, pharmacokinetics, pharmacodynamics, cholesterol, plaque, PCSK9, PCSK9 inhibitor therapy

RECEIVED: November 21, 2016. **ACCEPTED:** April 17, 2017.

PEER REVIEW: Three peer reviewers contributed to the peer review report. Reviewers' reports totaled 778 words, excluding any confidential comments to the academic editor.

TYPE: Original Research

FUNDING: The author(s) disclosed receipt of the following financial support for the research, authorship, and/or publication of this article: This study is funded by Sanofi and Regeneron.

DECLARATION OF CONFLICTING INTERESTS: The author(s) declared no potential conflicts of interest with respect to the research, authorship, and/or publication of this article.

CORRESPONDING AUTHOR: Karim Azer, Sanofi, 55 Corporate Drive, Bridgewater, NJ 08807, USA. Email: karim.azer@sanofi.com

Introduction

Increased plasma low-density lipoprotein cholesterol (LDL-C) is a risk factor for major cardiovascular disease.[1] Statin administration can result in significant reductions in cardiovascular mortality and morbidity.[1] However, some patients either do not respond adequately or cannot tolerate statins and would benefit from an alternative therapy. Proprotein convertase subtilisin/kexin type 9 (PCSK9) binds the low-density lipoprotein receptor (LDLR) and promotes degradation of the LDLR, leading to increased plasma LDL-C.[2,3] Alirocumab, a monoclonal antibody (mAb) that blocks PCSK9 binding to LDLR, leads to reduction in plasma LDL-C both when administered alone or in combination with other lipid-lowering therapies, including statins.[4–9] Of note, statin therapy leads to upregulation of PCSK9, and this could affect the LDL-C–lowering effect of alirocumab. In addition, patients with different underlying pathogeneses of hypercholesterolemia could have different responses to alirocumab and other lipid-lowering therapies.

To examine the mechanisms underlying responses to alirocumab and other lipid-lowering medications, we developed a quantitative systems pharmacology (QSP) model of whole-body cholesterol metabolism and plaque dynamics. Quantitative systems pharmacology models are an increasingly important approach for understanding the mechanism of drug effects by integrating disease biology, pharmacokinetic (PK) and pharmacodynamic data, and preclinical and clinical data.[10] There are several existing QSP models of cholesterol metabolism in the literature, which represent the relevant pathways in varying degrees of detail,[11–13] including one model which incorporates the PCSK9 pathway.[14] We describe in this article a QSP model that leverages existing models in the literature to predict the effects of lipid-lowering therapies on lipids and lipoproteins. The pathways that we chose to include in our model are connected to the mechanism of patient response to alirocumab, such as LDL-C and very low–density lipoprotein cholesterol (VLDL-C) internalization through LDLR, PCSK9-mediated degradation of LDLR, and exchange of cholesterol across cells and lipoproteins. Our model is novel in that it connects these pathways to a model of plaque formation so that we can use our model to understand the effect of alirocumab and other lipid-lowering therapies on cardiovascular risk.

We have developed 4 patient profiles for this model to exemplify the range of potential responses of patients being treated with statin or alirocumab therapy. Simulations of these 4 patient profiles allow us to test different treatment regimens to predict the range of cholesterol lowering achieved across the

patient phenotypes. On further refinement and calibration, our aim is to leverage the plaque dynamics in the model to predict the long-term effects of treatment. Preliminary results from the model are consistent with literature assessments of the effect of treatment on plaque volume and composition and could lead to new avenues for analysis in the future.

Methods

Model structure

The QSP model incorporates cholesterol metabolism and transport including LDLR trafficking, reverse cholesterol transport (RCT), sterol regulatory element–binding protein 2 (SREBP-2) regulation of cholesterol synthesis, LDLR expression, and PCSK9 expression. A depiction of the biology of PCSK9 and LDL, as well as the action of alirocumab is shown in Figure 1.[15] The model includes a representation of mechanistic hypotheses linking plasma LDL-C to atherosclerotic lipid core deposition, fibrosis, and inflammation in a representative coronary plaque. Treatments represented in the model include anti-PCSK9 antibody, statins, fibrates, and ezetimibe. The model consists of 74 species and corresponding ordinary differential equations (ODEs), 310 parameters, and 35 calculated outputs. (for model equations, see Supplementary Material). Model simulations for this article were run using the SimBiology toolbox of MATLAB (rel. 2016a, MathWorks, Inc., Natick, MA, USA).

The QSP model is an ODE model which simulates the behavior of lipoproteins, regulatory proteins, cholesterol, LDLR, plaque lipid and cellular components, and drugs localized in 5 main generalized areas within the body. These areas are represented as lumped compartments in the model; protein and cell levels are tracked separately for each compartment but are assumed to be well-mixed within each compartment. Compartments include plasma, gastrointestinal (GI) tract, hepatocytes, peripheral tissue, and plaque. The plasma and the GI tract are general representations, whereas hepatic and peripheral tissue cells contain subcompartments to describe intracellular, nuclear, and endosomal localizations within the cells. The plaque module incorporates the interplay between lipid and fibrotic processes, which in turn lead to changes in plaque volume.

Most reactions in the model are described by first-order mass action kinetics. These reactions are used to describe production or elimination of a model component or transfer of this component to a different compartment or form. For example, transfer of PCSK9 from the intracellular space of hepatocytes to plasma [$PCSK9_{icH \rightarrow pl}$] and formation of LDL-C from VLDL-C [$VLDL_{pl} \rightarrow LDL_{pl}$] are represented as follows:

$$\left[\mathrm{PCSK9}_{\mathrm{icH}\rightarrow\mathrm{pl}}\right] = PCSK9\_ic\_H\_to\_pl\_release\_rate\_k \cdot \mathrm{PCSK9}_{\mathrm{icH}}$$

$$\left[\mathrm{VLDL}_{\mathrm{pl}} \rightarrow \mathrm{LDL}_{\mathrm{pl}}\right] = VLDL\_to\_LDL\_conversion\_rate\_k \cdot \mathrm{VLDL\_pl}$$

The association of 2 proteins, such as the association of PCSK9 or LDL-C with the LDLR on the hepatic cell surface or in endosomes, is proportional to their product:

$$\left[\mathrm{PCSK9}_{\mathrm{pl}} + \mathrm{LDL-R} \rightarrow \mathrm{PCSK9{:}LDL-R}\right] = PCSK9\_LDLR\_pl\_association\_rate\_k \cdot \frac{PCSK9_{\mathrm{pl}} \cdot LDL-R}{Vol_{\mathrm{pl}}}$$

$$\left[\mathrm{LDL}_{\mathrm{en}} + \mathrm{LDL-R}_{\mathrm{en}} \rightarrow \mathrm{LDL{:}LDL-R}_{\mathrm{en}}\right] = LDL\_LDLR\_en\_association\_rate\_k \cdot \frac{LDL_{\mathrm{en}} \cdot LDL-R_{\mathrm{en}}}{Vol_{\mathrm{en}}}$$

The action of regulatory proteins such as SREBP-2 is represented through a Hill function. SREBP-2 controls intracellular production of both LDLR and PCSK9 in the same way:

$$\left[\mathrm{PCSK9}_{0\rightarrow\mathrm{icH}}\right] = PCSK9\_ic\_H\_production\_rate\_k \cdot \frac{SREBP2_{\mathrm{H}}^{n1}}{PCSK9\_EC50^{n1} + SREBP2_{\mathrm{H}}^{n1}}$$

$$\left[\mathrm{LDL-R}_{0\rightarrow\mathrm{icH}}\right] = LDLR\_ic\_H\_production\_rate\_k \cdot \frac{SREBP2_{\mathrm{H}}^{n2}}{LDL-R\_EC50^{n2} + SREBP2_{\mathrm{H}}^{n2}}$$

In this way, the maximum production rate is set and the reaction rate is decreased based on the level of SREBP-2 protein present. The impact of apolipoprotein A1 (apoA1) and apolipoprotein B (apoB) protein levels on high-density lipoprotein cholesterol (HDL-C) and VLDL-C formation, respectively, is also calculated in this way.

Drug administration in the model is designed to mimic clinical administration of the drug. Statin, ezetimibe, and fibrates are dosed orally once per day. Anti-PCSK9 antibodies are injected into a subcutaneous compartment on a once every 2 weeks or once every 4 weeks dosing schedule. The PK of statin, ezetimibe, and fibrate are each represented using compartmental PK models that approximate the clinically relevant drug exposure profiles. A Hill function of the effective drug concentration is used to model the pharmacodynamic impact of these drugs on reactions in the model. Pharmacokinetics of alirocumab are modeled using a target-mediated drug disposition (TMDD) framework. The pharmacodynamic impact of this drug is a result of the sequestration of free PCSK9 by the antibody.

In brief, the key actions represented within each compartment in the cholesterol metabolism model are as follows:

GI:

- Intake of food (represented as a constant source over the course of the day or as a discontinuous source present during 3 daily meals).

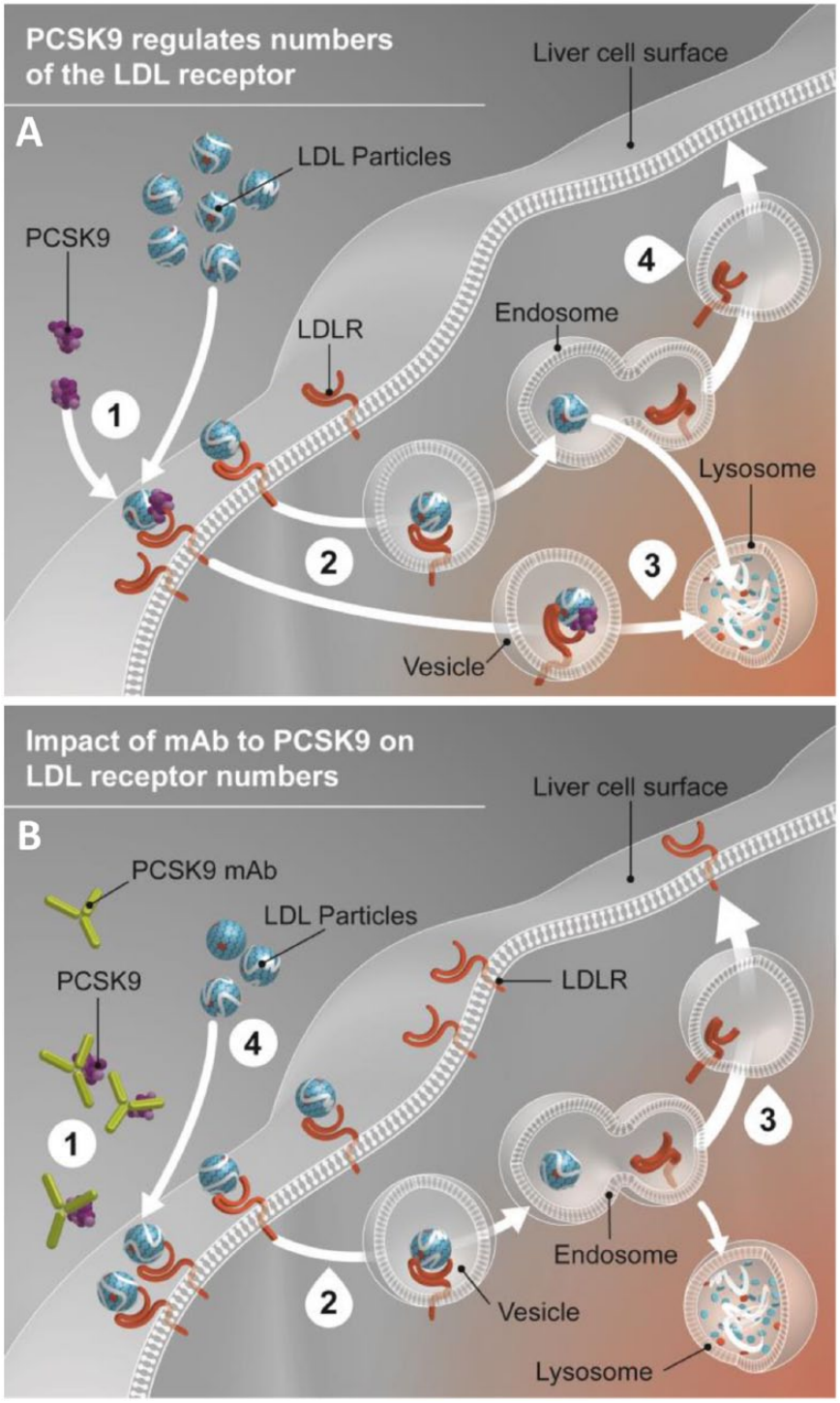

Figure 1. Role of PCSK9 in LDL metabolism and impact of PCSK9 monoclonal antibody. (A) (1) LDLR binds to LDL particle at the liver cell surface. PCSK9 can also bind to the LDLR. (2) The LDL particle-LDLR complexes with or without PCSK9 bound are internalized in the liver cell by endocytosis. (3) LDLR not bound to PCSK9 releases the LDL particle, which goes to a lysosome for digestion, whereas the LDLR is recycled to the cell surface. (4) LDLR bound to PCSK9 is digested in the lysosome along with the LDL particle. (B) (1) PCSK9 mAb binds PCSK9 in the circulation, preventing it from binding the LDLR. (2) The LDL particle-LDLR complexes are internalized in the liver cell. (3) In the absence of PCSK9 binding, LDLR recycling increases and more LDLRs bind to the liver cell surface as a result. (4) Circulating LDL particle levels are reduced. LDL indicates low-density lipoprotein; LDLR, low-density lipoprotein receptor; mAb, monoclonal antibody; and PCSK9, proprotein convertase subtilisin/kexin type 9. Reprinted with permission from Reyes-Soffer et al.[15] https://doi.org/10.1161/CIRCULATIONAHA.116.025253. Promotional and commercial use of the material in print, digital, or mobile device format is prohibited without the permission from the publisher Wolters Kluwer. Please contact healthpermissions@wolterskluwer.com for further information.

- Transfer of hepatic cholesterol to GI cholesterol pool.
- Elimination of cholesterol from food and from the GI cholesterol pool.
- Encapsulation of food and pooled GI cholesterol into chylomicrons.
- Transfer of chylomicrons to hepatic intracellular cholesterol pool through lymph.

Plasma:

- Secretion of VLDL-C (regulated by apoB), PCSK9, apoB, and apoA1 from hepatocytes into plasma.
- Transformation of VLDL-C to LDL-C.
- LDLR-independent clearance of PCSK9 from plasma.
- Binding of PCSK9, LDL-C, and VLDL-C to LDLRs on hepatocyte and peripheral cell surfaces.
- Direct internalization of LDL-C from plasma by hepatocytes and peripheral cells.
- Direct internalization of VLDL-C from plasma by hepatocytes.
- Production of HDL-C from excess cholesterol in peripheral cells and apoA1.
- Transformation of HDL-C cholesterol to LDL-C and VLDL-C cholesterol through RCT.
- Transport of drugs into and out of plasma.
- Binding of anti-PCSK9 mAb to PCSK9.

Hepatocytes:

- Production of intracellular cholesterol, mediated by activated SREBP-2.
- Transfer of cholesterol from cholesterol in the GI tract or chylomicrons in the lymph to intracellular cholesterol.
- Production of VLDL-C from intracellular cholesterol and secretion into plasma.
- Production of apoA1, apoB, LDLR, PCSK9, and SREBP-2 in the hepatic cell and trafficking of the first 4 of these proteins to the cell surface or plasma.
- Contribution of HDL-C, LDL-C, and VLDL-C directly to hepatic intracellular cholesterol.
- Uptake of VLDL-C through LDLR and contribution to intracellular cholesterol.
- Contribution of endosomal LDL-C to intracellular cholesterol.
- Internalization of LDL-C-LDLR and PCSK9-LDLR complexes from the cell surface into the endosome.
- Association and dissociation of PCSK9 and LDL-C from LDLR within the endosome.
- Elimination of endosomal LDLR and PCSK9, alone, or in a complex.

Peripheral cells:

- Production of intracellular cholesterol, mediated by activated SREBP-2.
- Production of LDLR and SREBP-2 in the peripheral cell nucleus and trafficking of LDLR to the cell surface.
- Direct contribution of LDL-C to hepatic intracellular cholesterol.
- Contribution of endosomal LDL-C to intracellular cholesterol.
- Uptake of VLDL-C through LDLR and contribution to intracellular cholesterol.
- Transfer of intracellular cholesterol to HDL-C in plasma through RCT.
- Internalization of LDL-C-LDLR and PCSK9-LDLR complexes from the cell surface into the endosome.
- Association and dissociation of PCSK9 and LDL-C from LDLR within the endosome.
- Elimination of endosomal LDLR and PCSK9, alone, or in a complex.

Aside from alirocumab, which acts only in the plasma by binding to PCSK9, other drugs act in different compartments of the model. A summary of the mechanisms of action represented for each drug are as follows:

- Fibrates inhibit transfer of HDL cholesterol to LDL-C and VLDL-C (RCT) and dissociation of LDL-C from LDLR on hepatocytes and peripheral cells. Fibrate promotes transport of hepatic intracellular cholesterol to the GI tract, transformation of VLDL-C into LDL-C, and production of apoA1 in hepatocytes.
- Ezetimibe inhibits cholesterol uptake in chylomicrons.
- Statins inhibit intracellular cholesterol production and promote production of apoA1 in hepatocytes.

Plaque model structure

The plaque model is an exploratory representation of mechanisms implicated in plaque formation and development. The plaque model includes a general pool of cells and LDL-C which contribute to plaque size and composition, which are mediated by cell apoptosis and inflammatory processes. First-order mass action equations are used to represent cell and protein production, degradation, and activation or oxidation. For processes which are influenced by the lumped effect of several biological mechanisms, such as the influence of activated cells on the level of inflammation, Hill functions are used. The volumes of plaque, its lipid core, and its fibrous core and cap are calculated by summing the contributions of the live and dead cells and cholesterol in the model. No drug is simulated to have a direct effect on the plaque, but plaque development is indirectly affected when LDL-C levels in plasma are reduced through treatment.

The main processes represented in the model are as follows:

- Low-density lipoprotein cholesterol entry to the plaque is facilitated by the activation of endothelial cells (ECs) lining the artery lumen.

- Low-density lipoprotein cholesterol in plaque is taken up by macrophages and smooth muscle cells (SMCs).
- Low-density lipoprotein cholesterol in plaque is oxidized and is taken up in this form by macrophages and SMCs.
- Macrophages and SMCs within the plaque can be activated and can become foam cells; all of these cells contribute to the lipid core of plaque.
- Excess cholesterol on SMCs and macrophages is transferred to HDL-C through RCT.
- All cell types may die, which is mediated by the level of inflammation, apoptosis, and cholesterol in the plaque.
- Inflammation is promoted by activated ECs, macrophages, SMCs, dead cells, and oxidized LDL-C.
- The lipid core of the plaque is formed by cholesterol carried on dead and live cells.
- The fibrous core and cap are produced by SMCs and degraded by matrix metalloproteinases (MMPs) produced by activated macrophages.
- Total plaque volume is a combination of lipid and fibrous cores and fibrous caps, as well as the volume added by circulating macrophages, SMCs, and foam cells in the plaque.

Model Calibration and Results

Overview

The goals of the lipid model were to develop a model incorporating whole-body lipid metabolism, effect of lipid-lowering therapies on lipid levels, and plaque dynamics. A schematic representation of the model is depicted in Figure 2. As an initial step in the development of the QSP model, a model was built to reproduce hepatic and peripheral lipid metabolism. Key lipid end points of interest included LDL-C, HDL-C, total cholesterol, non-HDL-C, and apoB concentrations. For hepatic lipid metabolism, key components included the following: (1) cholesterol input via synthesis, LDL-C/VLDL-C/HDL-C uptake, dietary intake, and enterohepatic circulation (EHC); (2) cholesterol output through VLDL-C and EHC; (3) effect of PCSK9 on LDLR internalization, degradation, and recycling; (4) hepatocyte production of PCSK9, LDLR, apoB, and apoA1, and (5) effect of intracellular cholesterol level on SREBP-2–regulated genes.

For peripheral lipid metabolism, key components included the following: (1) exchange of cholesterol between VLDL-C, LDL-C, and HDL-C in circulation; (2) peripheral cholesterol uptake through LDLR; (3) peripheral cholesterol production; (4) RCT; and (5) effect of intracellular cholesterol level on LDLR through SREBP-2. In addition, dietary cholesterol intake and EHC of biliary cholesterol were included in the model. The default parameterization of the model was calibrated to be representative of a statin-naïve patient with non–familial hypercholesterolemia (non-FH).[7]

Calibration of baseline model parameterization and virtual patients to represent therapeutic responses of interest

The QSP platform was developed and calibrated in JDesigner (Systems Biology Workbench, Inc., Claremont, CA, USA)[76] using published data in accordance with Rosa's Model Qualification Method.[16,65] The base parameterization of the model, VP0, is representative of a statin-naïve patient with non-FH as described in the phase 3 study published by Roth et al.[7] Initial parameter values were obtained from animal and clinical studies in the literature (see Supplementary Table 1 for full list of parameter descriptions and references/guidelines used for initial estimates). Many values were taken from an existing model of cholesterol metabolism which does not include PCSK9.[11] Known biological constraints were also used to guide the baseline parameterization, such as the relative affinity of LDL-C and PCSK9 for LDLR in neutral (at the cell surface) vs acidic (endosomal) pH, the approximate half-life of LDLR, and the synthesis rate and pool size of PCSK9 in plasma. Parameters were adjusted to achieve physiologically relevant cholesterol/lipid values and dynamics.

Because the model is fairly large and encompasses representations of many biological subsystems, calibration of smaller modules was done before calibration of the final model output was performed. Calibration of the functions used to model the effect of intracellular cholesterol on relative endoplasmic reticulum (ER) cholesterol, relative SREBP-2 activation, and relative SREBP-2–regulated expression is shown in Figure 3.

Once the biological parameter values were established for the base calibration, the model was further calibrated to reproduce the effects of established cholesterol-lowering therapies (statins, ezetimibe, and fibrates) as well as the newly emerging class of PCSK9 inhibitors, exemplified by the mAb alirocumab. Known PK parameters for statin therapy were taken from package inserts and the literature.[19,20] We included known mechanisms of action for statins, ezetimibe, and fibrates into the model and calibrated the parameters influencing the pharmacodynamic effect of each drug to the average clinical response across clinical trial data reported in the literature.[5,20–24]

Alirocumab administration was modeled using TMDD PK. To calibrate the qualitative response to anti-PCSK9 therapy, clinical studies describing patient response to alirocumab were evaluated.[5,6] The key mechanism for anti-PCSK9 mAbs was prevention of PCSK9-mediated targeting of LDLR to lysosomes through mAb-PCSK9 immune complex formation and clearance. Results of clinical trials evaluating the PK profile and efficacy in lowering LDL-C, kinetics, and magnitude of the LDL response and responses of other lipoproteins were assessed in the optimization.

As a part of the model calibration, we also created representative virtual patients (VPs) to match the phenotype of patients enrolled in a clinical study with alirocumab. Each VP

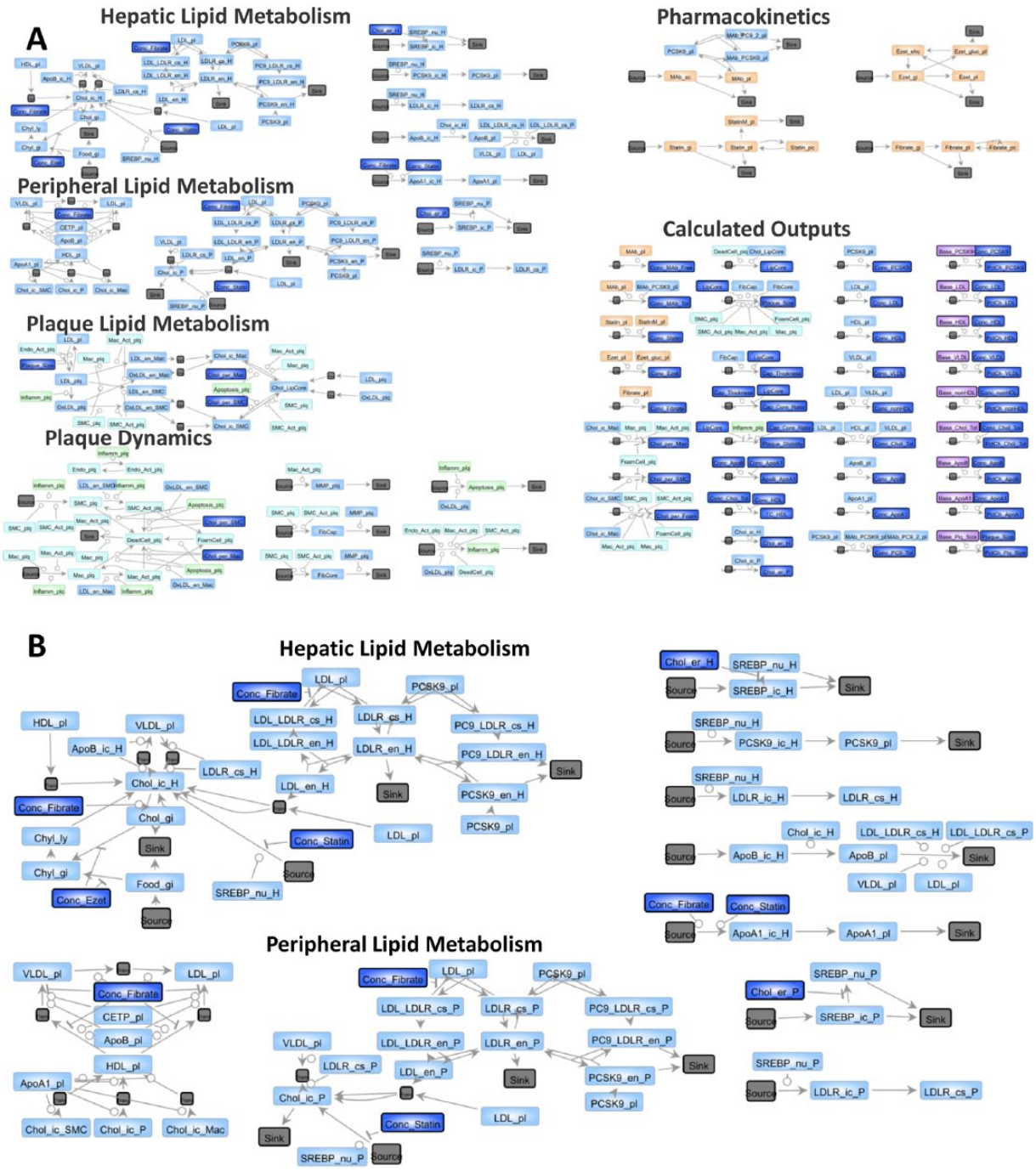

Figure 2. Schematic representation of cholesterol metabolism QSP model: a depiction of the model from PhysioPD is shown. Subsections of the models are labeled. The entire model is shown in (A) and a close up of the hepatic and peripheral subsections where PCSK9 acts is shown in (B). Colors indicate different model components, including cells (light blue), species (ie, proteins and metabolites, blue), treatments (orange), processes (green), sources/sinks (gray), and outputs (purple).

is a complete parameterization of the model that represents a specific balance of biological mechanisms which leads to a given clinical phenotype. The final subset of parameters that were chosen to define the differences between the VPs (Table 2) provided handles to explore hypotheses related to the function of these mechanistic pathways. During the calibration procedure, the parameters were adjusted in JDesigner to achieve the desired VP characteristics. A set of VPs were defined by selecting key physiological pathways affecting processes that are known to vary in cardiovascular disease. Parameter scans were performed in JDesigner to determine which parameters in these pathways were best able to modulate the therapy outcomes. Literature sources and guidelines used to initialize these parameters are cited in Table 1. Parameters were manually adjusted to identify VPs (parameterizations of the model) who showed high or low response to simulation of statin or alirocumab treatment. For alirocumab treatment, the model was calibrated so that the responder profile exhibited a

Table 1. Parameter values adjusted to create VPs representing varied response to statin and alirocumab therapy.

PROCESS	PARAMETER	VP0	VP1	VP2	VP3	VP4	UNIT	REFERENCE/CALCULATION
Rate of bile salt entering GI	Bile_acid_chol_secretion_rate_k	0.0143	0.01235	0.0135	0.011	0.017	1/h	Adjusted to achieve desired baseline LDL
Hepatic cholesterol synthesis	Chol_ic_H_production_rate_k	70000	100000	40000	70000	40000	nmol/h	Adjusted to represent high or low cholesterol synthesis
Hepatic unbound LDLR degradation rate	LDL-R_en_H_degradation_rate_k	0.035	0.035	0.035	0.02	0.08	1/h	Estimated from LDLR turnover rate
Peripheral unbound LDLR degradation rate	LDL-R_en_P_degradation_rate_k	0.035	0.035	0.035	0.02	0.08	1/h	Estimated from LDLR turnover rate
LDLR synthesis rate, hepatocytes	LDL-R_ic_H_production_rate_k	2	2.9	1.8	2.4	1.56	nmol/h	Calculated to balance LDLR turnover rate
LDLR synthesis rate, peripheral	LDL-R_ic_P_production_rate_k	0.7	0.9	0.6	0.8	0.5	nmol/h	Calculated to balance LDLR turnover rate
PCSK9 synthesis	PCSK9_ic_H_production_rate_k	3.5	3.5	3.5	3.1	5	nmol/h	Based on clearance and steady-state amount in plasma[25]
Affinity of PCSK9 for LDLR at acidic pH	PCSK9_LDL-R_en_Kd	10	10	10	5	20	nM	Cunningham et al[26] and Piper et al[27]
Affinity of PCSK9 for LDLR at neutral pH	PCSK9_LDL-R_pl_Kd	350	350	350	175	700	nM	Cunningham et al[26] and Piper et al[27]
PCSK9 clearance	PCSK9_pl_clearance_rate_k	0.1	0.1	0.1	0.05	0.3	1/h	Adjusted to achieve desired PCSK9 level
Transfer of cholesterol from HDL to VLDL	HDL_to_VLDL_exchange_rate_k	0.0158	0.0238	0.0238	0.0238	0.0238	1/h	Calculated based on Giugliano et al[28] and McAuley et al[11]
Transfer of cholesterol from HDL to LDL	HDL_to_LDL_exchange_rate_k	0.0017	0.0026	0.0026	0.0026	0.0026	1/h	Calculated based on Giugliano et al[28] and McAuley et al[11]
Hill coefficient for SREBP-2–regulated PCSK9 synthesis	SREBP_PCSK9_nh	4	2	4	4	4	Unitless	Adjusted to provide varying degrees of response to SREBP-2 activation
Hill coefficient for SREBP-2–regulated LDLR synthesis	SREBP_LDL-R_nh	4	4	3	4	4	Unitless	Adjusted to provide varying degrees of response to SREBP-2 activation

Abbreviations: GI, gastrointestinal; HDL, high-density lipoprotein; LDL, low-density lipoprotein; LDLR, low-density lipoprotein receptor; PCSK9, proprotein convertase subtilisin/kexin type 9; SREBP-2, sterol regulatory element–binding protein 2, VP, virtual patient.
VPs 1 and 2 are statin responders and nonresponders, respectively. VPs 3 and 4 are alirocumab responders and nonresponders, respectively.

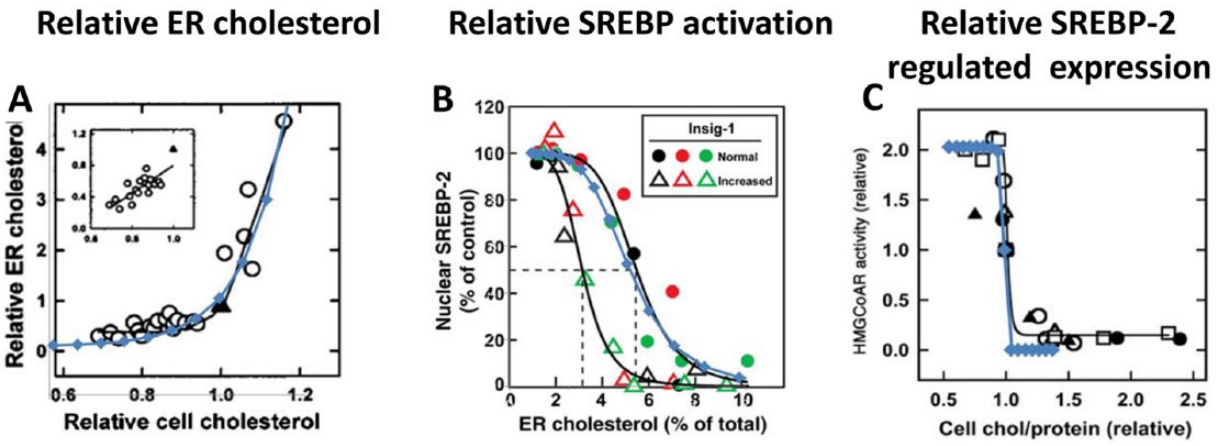

Figure 3. ER cholesterol levels and subsequent SREBP-2–regulated response as a function of changes in total cellular cholesterol: (A) Relative ER cholesterol as a function of relative total cellular cholesterol as measured by Lange et al[17] along with the corresponding exponential fit (blue) used to define ER cholesterol levels in the platform. (B) Hill function fit (blue line) that provides an appropriate response of SREBP-2 activation to relative changes in ER cholesterol. The graph represents the combined data from experiments where cholesterol was delivered by cyclodextrin complexes (cholesterol/MCD) (red and green symbols) and experiment (black symbols) where cholesterol was delivered by β-VLDL to CHO cells. (C) HMG CoA reductase activity as a function of relative total cellular cholesterol as measured by Lange et al[18] along with the corresponding Hill function fit (blue) used to define SREBP-2 response to changes in cellular cholesterol levels in the platform. HMG CoA reductase gene expression is regulated by SREBP-2. CHO indicates Chinese hamster ovary; ER, endoplasmic reticulum; HMG CoA; 3-hydroxy-3-methylglutaryl coenzyme A; MCD, methyl-β-cyclodextrin; SREBP-2, sterol regulatory element–binding protein-2.

Table 2. Baseline characteristics of VPs with statin background therapy prior to therapy.

CHOLESTEROL	VP0	VP1	VP2	VP3	VP4
LDL, mg/dL	145	169	168	170	169
Total cholesterol, mg/dL	223	241	239	242	239
ApoB-100, g/L	1.15	1.25	1.25	1.25	1.28
HDL, mg/dL	55.0	46.3	46.2	46.3	46.0
VLDL, mg/dL	23.7	25.5	25.1	25.6	24.6
Non-HDL-C, mg/dL	168	195	193	196	193
PCSK9					
Free	3.3 nM (238 ng/mL)	3.0 nM (216 ng/mL)	4.5 nM (324 ng/mL)	1.8 nM (130 ng/mL)	4.7 nM (338 ng/mL)
Plaque					
Plaque volume, mm^3	78	85	84	84	84
Lipid core, mm^3	31	38	37	37	37

Abbreviations: ApoB, apolipoprotein B; HDL, high-density lipoprotein; HDL-C, high-density lipoprotein cholesterol; LDL, low-density lipoprotein; VLDL, very low–density lipoprotein; PCSK9, proprotein convertase subtilisin/kexin type 9; SREBP-2, sterol regulatory element–binding protein 2, VP, virtual patient.
VP0 is the baseline platform parameterization, representative of a statin-naïve patient with non-FH.[7] VPs 1 and 2 are statin responders and nonresponders, respectively. VPs 3 and 4 are alirocumab responders and nonresponders, respectively.

75% reduction in LDL-C after treatment, and the nonresponder profile had a 17% reduction in LDL-C. The calibrated values of key parameters determined for each VP are shown (Table 1), as well as the resulting baseline values of each patient (Table 2).

An analysis of the calibration results shows that some parameters were highly variable across all VPs, including the rate of bile salt entering the GI tract, the rate of hepatic cholesterol de novo synthesis, and the rate of LDLR synthesis. The only additional difference between statin responders and nonresponders in the model was the steepness of the effect of SREBP-2 level on LDLR and PCSK9 synthesis. Alirocumab responsive and nonresponsive patients differed significantly in their rate of unbound LDLR degradation, rate of PCSK9 synthesis, affinity of PCSK9 for LDLR, and rate of independent PCSK9 clearance. With this insight gained from the initial model fitting, these values could be compared with data on lipoprotein and PCSK9 levels from clinical trials, and data on

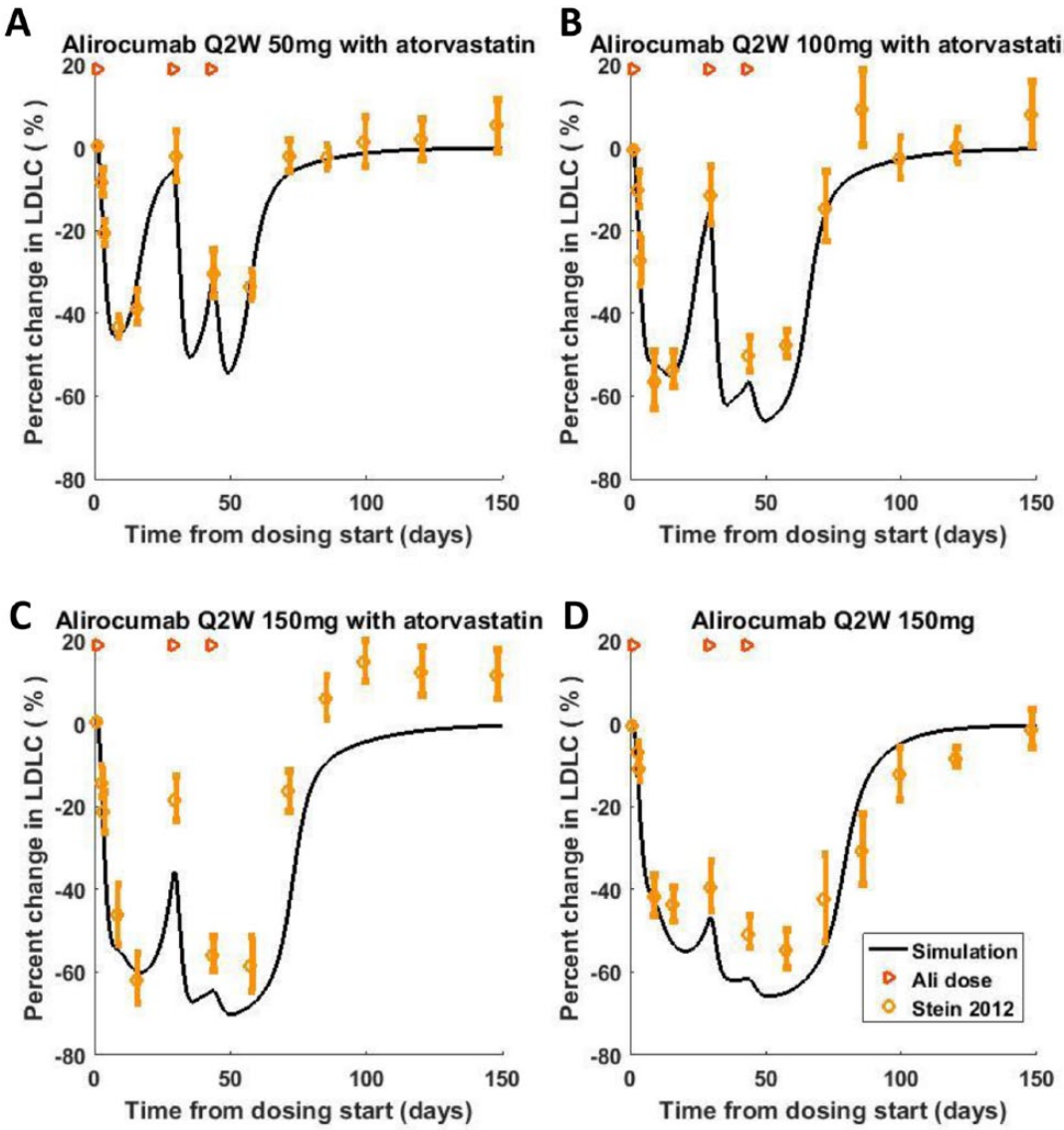

Figure 4. Calibration of cholesterol model to clinical studies: data from Stein et al[4] were used to calibrate the model for patients with non-familial hypercholesterolemia. Comparison of simulation of multiple doses of (A) 50 mg, (B) 100 mg, or (C and D) 150 mg alirocumab on days 1, 29, and 43 for a typical virtual patient. For plots (A-C), model was run to steady state (4000 hours) with 10 mg statin therapy every day before alirocumab was administered, to simulate statin background of patients enrolled in clinical trial. Plot (D) shows data from patients on diet therapy alone at the start of treatment, so background statin therapy was not simulated. Simulated effect of alirocumab on LDL-C for typical virtual patient on statin background shown as lines, data are shown as single points representing mean and standard deviation of patient group at each time point. Time of alirocumab administration is indicated by the orange arrow at the top of the figure. Percent change is calculated from first day of alirocumab treatment. VP2 parameterization was used for both simulations. LDL-C indicates low-density lipoprotein cholesterol.

variability in lipoprotein and PCSK9 synthesis and clearance in tracer kinetics studies[29] to assess whether the parameter values in these VP profiles are reasonable and to more systematically optimize them.

Simulations to qualify calibration of QSP model for statin and alirocumab treatments

To ensure that clinical outputs predicted by the model were in line with clinical data, calibration of the baseline parameterization of the model to published clinical studies was performed. We calibrated the model to a clinical study which examined the effect of multiple doses of alirocumab on patients with familial hypercholesterolemia or non-FH on a stable atorvastatin dose or on diet therapy alone[4] (Figure 4). Patients received an alirocumab dose of 50, 100, or 150 mg on days 1, 29, and 43 of the trial. In another cohort of the study, patients were administered the same schedule of 150 mg alirocumab but without statin therapy. To replicate this study, we simulated a typical VP on statin background by running the model with 10 mg statin every day until a steady state was reached. Patients not receiving statin in the study were run for the same initialization period without treatment. At this point, alirocumab was given 150 mg on the designated study days. We demonstrate that the

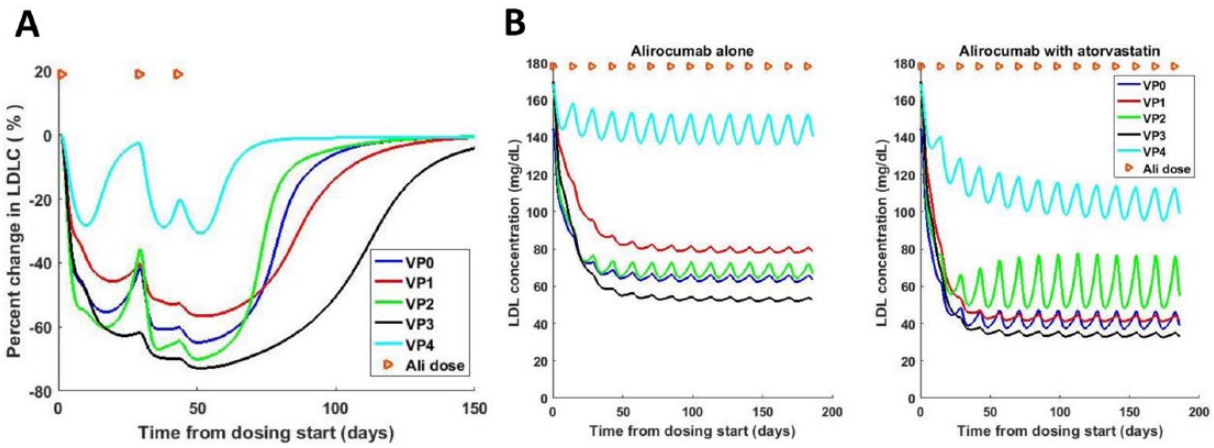

Figure 5. Use of model to predict range of patient responses to different therapy combinations: simulations run for VPs 0 to 4 using same treatment regimen. (A) Simulation of Stein et al[4] multiple dosing protocol of alirocumab 150 mg on days 1, 29, and 43 for patients on a background of 10 mg statin. Simulations of VPs on statin therapy alone were run for 4000 hours before alirocumab dose was started. Percent change is calculated from baseline value prior to first dose of alirocumab treatment. (B) Simulation of 75 mg alirocumab given once every 2 weeks to each VP, alone (left panel) or in combination with 40 mg statin (right panel), all daily. VP legend: VP0 (dark blue), VP1 (red), VP2 (green), VP3 (black), VP4 (light blue). Time of alirocumab administration is indicated by the orange arrows at the top of the figure. LDL-C indicates low-density lipoprotein cholesterol; VP, virtual patient.

same parameterization of the model reflects a similar degree of reduction in LDL-C induced by multiple doses of alirocumab therapy, and that the model is calibrated to accurately simulate the effects of combination therapy with both alirocumab and statin. Overall, simulations conducted with the model replicated many key features of cholesterol metabolism, similar to observations from clinical studies with lipid-lowering therapies (Figures 4 to 6).

By running simulations with the different VP profiles, the model can be used to simulate a range of patient responses to different cholesterol-lowering therapies. When the simulation is run to replicate the multiple dosing schedule of 150 mg alirocumab in a phase 1 study,[4] a range of patient responses to treatment is observed for each VP (Figure 5A). The maximum reduction in LDL-C level achieved in VPs 0 to 3 (baseline patient, statin responder, statin nonresponder, and alirocumab responder, respectively) falls between 56% and 73%. All patients return to their baseline LDL-C level when alirocumab treatment is stopped, but the dynamics of how quickly patients return to baseline differs; VP3, whose profile is most responsive to alirocumab, retains low LDL-C levels (within 5% of baseline) for 103 days after the cessation of treatment (146 days from baseline). VP4 represents a patient with suboptimal response to alirocumab treatment. The LDL-C of VP4 is reduced by 31% at maximum, and LDL-C levels increase to within 5% of baseline within 24 days of the last treatment (67 days from baseline). This finding underscores that the average patient response reported is composed of heterogeneous groups of patients who have different responses to alirocumab treatment.

This model can be used to aid in prediction of which combination therapies might be optimal for patients. Figure 5B shows a simulation of alirocumab given alone (left panel), in comparison with alirocumab given in combination with statin (right panel). The degree of response to alirocumab among the

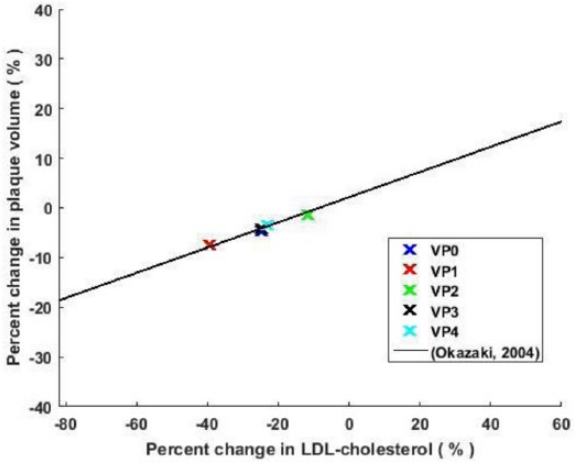

Figure 6. Calibration of plaque model to clinical studies: Plot of simulated and clinically measured percent change in LDL-C vs percent change in plaque volume. Simulations run to replicate dosing scheme used in Okazaki et al,[30] where patients were given 20 mg atorvastatin every day for 6 months. Simulations for each VP are shown as points. Line depicts line fit to clinical measurements for patients with baseline LDL-C > 125 mg/dL in Okazaki et al.[30] Change in plaque and LDL size is compared with level of both at baseline before the start of treatment. LDL, low-density lipoprotein; LDL-C indicates low-density lipoprotein cholesterol; VP, virtual patient.

VPs generally remains the same across the treatments, with VP3 showing the greatest LDL reduction and VP4 showing the least reduction. However, the simulations can provide some information about effects of combination therapies for the different VPs. In the simulations, all VPs seem to show a greater extent of LDL reduction when alirocumab is combined with statin (Figure 5B, right panel) compared with alirocumab alone, and indeed, patients VP0 and VP1 have a similar response in this regimen to the alirocumab high responder patient. As is expected, VPs 2 and 4 (statin and alirocumab low

responders, respectively) do not show as great a reduction in LDL-C with this dosing combination. The variation in response to treatment between the VPs highlights the importance of the underlying biology of the patients that they represent, and that this affects the degree of LDL-C reduction (see further analysis of this subject in McQuade et al[31]). As more drugs are developed or new patient types are identified, this model is a valuable tool for exploring dosing regiments before embarking on testing in the clinic.

Plaque calibration

To better understand the consequences of changes in the lipid profile, a QSP model of plaque dynamics was developed. To reproduce plaque dynamics, the model aimed to reproduce plaque lipid metabolism and trafficking and processes leading to plaque formation and reversal with appropriate therapy. Key components of the lipid metabolism in the plaque model included the following: (1) localization of LDL-C to the plaque lesion and subsequent production of modified (eg, oxidized) LDL-C, (2) LDL-C uptake by macrophages and SMCs, and (3) formation of an acellular lipid core. In the plaque model, cell types included the following: (1) plaque cellular components (eg, monocytes/macrophages, SMCs, ECs, foam cells) and (2) cells involved in hepatic and peripheral cholesterol and PCSK9 production and clearance (eg, hepatocytes, ECs). Critical cell-related elements of the plaque dynamics model included the following: (1) EC activation (with positive feedback through inflammatory pathways); (2) macrophage recruitment/proliferation, activation, and foam cell formation; (3) cell death and removal of cellular debris by macrophages; (4) SMC recruitment/proliferation and activation and foam cell formation; (5) production of MMPs; (6) formation of a lipid core and fibrous cap; and (7) contribution of inflammatory and apoptotic processes. Changes in plaque size and composition were assessed by examining plaque size and percentage change in size.

Guidelines for plaque calibration were taken from in vitro studies with human cell lines and clinical studies and are summarized in Table 3. Because plaque is more difficult to measure than LDL-C, which can be obtained from a blood sample, there have been fewer human studies measuring plaque, and findings are not as clear and consistent. Data obtained from a report of plaque volume changes in statin-naïve patients with hypercholesterolemia with a history of acute coronary syndrome[30] were used to calibrate the plaque component of the model (Figure 6). The treatment regimen given in this study, 20 mg atorvastatin therapy every day more than 6 months, was simulated for each VP profile. Comparing predictions of the model for each VP with the line fit in Okazaki to patient data for patients with baseline LDL-C > 125 mg/dL, we see that all VPs fall very close to this line describing average relationship of change in LDL-C to change in plaque (Figure 6). The plaque model is complex, and not all processes involved in plaque remodeling are well understood biologically. Therefore, this model should be considered as an initial attempt to connect cholesterol changes to cardiovascular outcomes, but it must be more completely developed and further qualified before it is used to reliably predict plaque changes. New data that emerge from future clinical studies could be used for calibration.

The plaque model can be used to give novel insight on the effect of treatments on plaque size and composition

A QSP model of plaque development can be extremely valuable to gain insight on mechanisms affecting long-term outcomes of cholesterol treatment. Our model is developed to predict not only the overall plaque volume changes but also the changes in plaque composition. Changes in fibrotic and lipid components of the plaque arise from different processes and thus have different responses to therapy. The lipid core of the plaque is formed through deposition of cholesterol by oxidized or plaque-localized LDL and by apoptotic macrophages and SMCs. Cholesterol from the lipid core can also be taken up by cells within the plaque and shuttled to HDL via the RCT pathway. The fibrotic portion of the plaque consists of 2 components, a fibrotic core surrounded by a fibrotic cap, thus differentiating the fibrotic surface portion of the plaque at the vessel lumen (the cap) from the fibrotic material inside the plaque. Both the fibrotic core and cap are constructed similarly: formed through deposition of fibrotic components by SMCs in the plaque and degraded by MMPs.

Our initial model of plaque suggests an interesting interplay between fibrotic and lipid core components of the plaque that could affect whether overall plaque volume increases or decreases. In a simulation with alirocumab therapy given to patients with initially high LDL-C levels on 80 mg statin background, a large reduction in lipid core size counteracts a gain in fibrotic volume to lead to an overall reduction in plaque volume (Figure 7B). However, in patients with initially low LDL-C, an initial overall gain in plaque volume may occur due to the increase in fibrotic core and cap size in combination with a relatively lower reduction in volume of lipid core, potentially reflecting the lower baseline lipid core volume (Figure 7A). This is consistent with some reports showing that the lipid core decreases in response to treatment, whereas the fibrotic portion of the plaque increases in size or remains the same.[36,56,57] The size of the lipid core component of plaque is correlated with negative outcome, but the fibrotic cap thickness is suggested to protect the plaque from rupture.[58] This aspect of the model suggests an interesting prediction for further validation and analysis and suggests that clinical studies of plaque should study both plaque composition and overall plaque volume to obtain a true picture of the benefit of treatment.

Table 3. Baseline plaque characteristics and target criteria for calibration.

CHARACTERISTIC	BASELINE CV PLATFORM	TARGET CRITERIA	REFERENCES
Plaque location	Coronary vessel (4 mm diameter)	Coronary vessel (4 mm diameter)	Dodge et al[32] and Yamagishi et al[33]
Plaque volume, mm^3	69 (assuming 10-mm lesion length for analysis), 55% stenosis	62.5-75 (based on 50%-60% stenosis)	Sipahi et al[34]
Lipid core, %	32	20-40	Varnava et al,[35] Hattori et al,[36] and van Gils et al[37]
Cap thickness, mm	0.14	0.05-0.15	Hattori et al[36]
Cellular composition	Mac: 7%, SMC: 3%	Mac: 3%-40% plaque area, SMC: 3%-50% plaque area	Davies et al,[38] Kolodgie et al,[39] Moreno et al,[40] Nakata et al,[41] Tanaka et al,[42] Tearney et al,[43] van der Wal and Becker,[44] and Virmani et al[45]
Cellular proliferation vs recruitment	Mac: 58% proliferation, SMC: 10% proliferation	Mac: 30%-80% proliferation, SMC: 3%-14% proliferation	Bennett et al,[46] Katsuda et al,[47] Lutgens et al,[48] and Robbins et al[49]
LDL permeability, mm/h	0.036 (maximum)	$2\times10^{-7}-1\times10^{-6}$ cm/s (0.0072-0.036)	Cancel and Tarbell[50,51]
LDL oxidation, 1/h	~0.1 (modulated by the level of inflammatory signaling)	Oxidation half-life of several hours observed in vitro	Di Tomaso et al,[52] Karner and Perktold,[53] and Sun et al[54]
Reverse cholesterol transport	$1\times10^{-4}-1\times10^{-3}$ 1/h (750 mg/d RCT from periphery)	~700-900 mg/d RCT from periphery	McAuley et al[11]
% macrophages, smooth muscle cells % activated cells	Mac: 28% of all cells, SMC: 38% of all cells, activated Mac, 21% of Mac, activated SMC, 13% of SMC	Mac: 10%-50% of all cells, SMC: 20%-50% of all cells, % activated cells: 5%-30% (may be higher for unstable plaques)	Kolodgie et al,[39] Lutgens et al,[48] van der Wal and Becker,[44] and Varnava et al[35]
Foam cell formation	Mac: 78%, SMC: 22%	~20%-40% derived from SMC (may be higher in advanced lesions)	Li et al[55] and Nakata et al[41]

Abbreviations: LDL, low-density lipoprotein; Mac, macrophages; SMC, smooth muscle cell.

Discussion

Alirocumab is a novel therapy for treating hypercholesterolemia by inhibiting PCSK9 activity. To better understand the role of PCSK9 in lipid biology and the biologic effects of alirocumab treatment, we have developed a QSP model of lipid metabolism, including interactions and regulation of PCSK9, LDLR, LDL-C, and other components of lipid metabolism. In examining the impact of alirocumab administration and assessing potential effects on plaque dynamics, this model extends previously described QSP models on cholesterol metabolism.[11,14] The effects of alirocumab both with and without concomitant statin therapy were explored in the model. In addition, a model simulating the effects of changes in LDL-C on plaque dynamics was also developed.

The cholesterol metabolism model structure and parameters were based on both clinical and preclinical data and calibrated to data from clinical trials with alirocumab. Qualification of the model was performed by confirming that changes in LDL-C, HDL-C, total cholesterol, and apoB predicted by the model in response to alirocumab treatment matched data from an independent clinical trial with alirocumab. This confirmed that the key components of the model reflecting interactions and regulation of PCSK9 and the LDLR with consequent effects on LDL-C and other lipoproteins were accurately represented.

Although the pathways involved in the cholesterol metabolism model are well established, the mechanisms involved in plaque formation are not as definite. Our plaque model was developed to represent the cells and factors with a recognized role in plaque formation in a semimechanistic way. Our model assumes that the key link between cholesterol metabolism and plaque development is the amount of LDL-C in the plasma, which has been demonstrated in the literature.[59] We also incorporate cholesterol transfer from macrophages and SMCs in plaque to apoA1 to form HDL-C through the RCT pathway.[60] We chose not to emphasize the influence of HDL-C level on plaque formation in the model due to contradictory studies in animals and clinical trials which demonstrate that the mechanisms controlling the relationship of HDL-C to cardiac outcomes are not straightforward.[60-62]

In this model, simulations of studies with patients with hypercholesterolemia were based on a representative VP, and VPs reflecting differential response to lipid-lowering therapies were developed. Future efforts will be directed to developing a

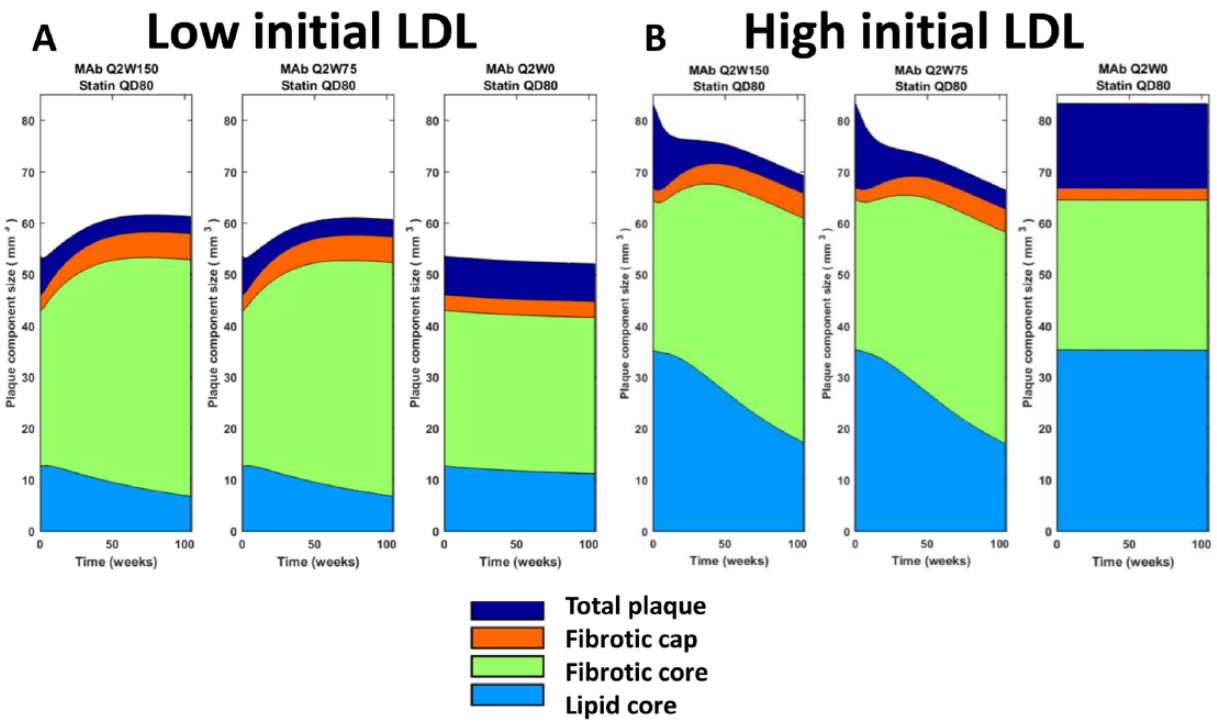

Figure 7. Plaque model can simulate changes in both plaque size and composition: the rate of hepatic cholesterol production was altered in the model to create virtual patients with initially (A) low and (B) high LDL levels and plaque sizes. Models were run to steady state on background with 80 mg statin therapy every day. Sizes of plaque, fibrotic cap, core, and lipid core are outputs from the model and are colored as shown in the legend. In both (A) and (B), alirocumab dose given on top of statin is 150 mg once every 2 weeks, 75 mg once every 2 weeks, and none (statin treatment only), from left to right panel, respectively. LDL indicates low-density lipoprotein.

greater range of different VPs to reflect the heterogeneity of the patient population receiving lipid-lowering therapies. These VPs could be constructed to show the differences in underlying biology that gives rise to the dyslipidemia, even in patients who have similar circulating levels of the lipoproteins. These VPs will lead to a greater understanding of the mechanisms underlying the differences in clinical response to different lipid-lowering treatments. For example, even for patients with the same initial LDL-C level, some may show a greater clinical response to alirocumab or other treatments than others, and the QSP model may be very useful for understanding and generating hypotheses about the underlying physiologic reasons for the difference in response. Parameterizations of the model could also be developed to represent patients from different disease subgroups with increased risk of dyslipidemia, such as patients with diabetes mellitus.

A further extension of the model would be to examine the effect of alirocumab on other lipoproteins. Alirocumab has been observed to have effects on lipoprotein(a), apoA1, and triglycerides.[9,63] A more complete understanding of the physiologic basis of the effects of alirocumab could also lend insight into potential biomarkers that may predict which patients will show clinical benefit from alirocumab.

For the plaque portion of the model, by including various cell types and processes involved in plaque formation and development, simulations of the model were able to qualitatively reflect the effect of changes of plaque volume over time in the setting of reduction in LDL-C. As the risk of plaque rupture and clinical sequelae depend not only on plaque size but also on plaque composition, future studies will examine in more detail the evolution of both plaque size and composition at different time points following lipid-lowering therapies. In addition, the model can be used to probe for potential biomarkers predicting benefit to alirocumab therapy.

In summary, the QSP model of PCSK9, LDL-C, and other lipids can lead to an enhanced understanding of the effects of alirocumab and lend insight into the potential effects governing differential response to treatment and effects on plaque dynamics.

Acknowledgements

The authors would like to thank Aurelie Brunet, Uwe Schwahn, Bernard Sebastien, and Werner Seiz for input on the model development and Kevin Rodden for his discussion on the plaque representation in the model.

Author Contributions

JEM, DWB, KA, and TN conceived and designed the experiments. JEM, DWB, KA, TN, and JE analyzed the data. JEM, REA, and KA wrote the first draft of the manuscript. JEM, REA, KA, and DWB contributed to the writing of the manuscript. All authors agree with manuscript results and conclusions. JEM, REA, and KA jointly developed the structure and arguments for the paper. All authors made critical revisions and

approved final version. All authors critically reviewed and approved the final manuscript.

Disclosures and Ethics

As a requirement of publication, author(s) have provided to the publisher signed confirmation of compliance with legal and ethical obligations including but not limited to the following: authorship and contributorship, conflicts of interest, privacy and confidentiality, and (where applicable) protection of human and animal research subjects. The authors have read and confirmed their agreement with the ICMJE authorship and conflict of interest criteria. The authors have also confirmed that this article is unique and not under consideration or published in any other publication, and that they have permission from rights holders to reproduce any copyrighted material. Any disclosures are made in this section. The external blind peer reviewers report no conflicts of interest.

REFERENCES

1. Baigent C, Blackwell L, Emberson J, et al. Efficacy and safety of more intensive lowering of LDL cholesterol: a meta-analysis of data from 170,000 participants in 26 randomised trials. *Lancet*. 2010;376:1670–1681.
2. Seidah NG, Benjannet S, Wickham L, et al. The secretory proprotein convertase neural apoptosis-regulated convertase 1 (NARC-1): liver regeneration and neuronal differentiation. *Proc Natl Acad Sci U S A*. 2003;100:928–933.
3. Abifadel M, Varret M, Rabès JP, et al. Mutations in PCSK9 cause autosomal dominant hypercholesterolemia. *Nat Genet*. 2003;34:154–156.
4. Stein EA, Mellis S, Yancopoulos GD, et al. Effect of a monoclonal antibody to PCSK9 on LDL cholesterol. *N Engl J Med*. 2012;366:1108–1118.
5. Roth EM, McKenney JM, Hanotin C, Asset G, Stein EA. Atorvastatin with or without an antibody to PCSK9 in primary hypercholesterolemia. *N Engl J Med*. 2012;367:1891–1900.
6. McKenney JM, Koren MJ, Kereiakes DJ, Hanotin C, Ferrand AC, Stein EA. Safety and efficacy of a monoclonal antibody to proprotein convertase subtilisin/kexin type 9 serine protease, SAR236553/REGN727, in patients with primary hypercholesterolemia receiving ongoing stable atorvastatin therapy. *J Am Coll Cardiol*. 2012;59:2344–2353.
7. Roth EM, Taskinen MR, Ginsberg HN, et al. Monotherapy with the PCSK9 inhibitor alirocumab versus ezetimibe in patients with hypercholesterolemia: results of a 24 week, double-blind, randomized Phase 3 trial. *Int J Cardiol*. 2014;176:55–61.
8. Cannon CP, Cariou B, Blom D, et al. Efficacy and safety of alirocumab in high cardiovascular risk patients with inadequately controlled hypercholesterolaemia on maximally tolerated doses of statins: the ODYSSEY COMBO II randomized controlled trial. *Eur Heart J*. 2015;36:1186–1194.
9. Robinson JG, Farnier M, Krempf M, et al. Efficacy and safety of alirocumab in reducing lipids and cardiovascular events. *N Engl J Med*. 2015;372:1489–1499.
10. Sorger PK, Allerheiligen SRB, Abernethy DR, et al. Quantitative and systems pharmacology in the post-genomic era: new approaches to discovering drugs and understanding therapeutic mechanisms. In: Ward R, ed. *An NIH White Paper by the QSP Workshop Group*. Bethesda, MD: NIH; 2011: 1–48.
11. McAuley MT, Wilkinson DJ, Jones JJ, Kirkwood TB. A whole-body mathematical model of cholesterol metabolism and its age-associated dysregulation. *BMC Syst Biol*. 2012;6:130.
12. Lu J, Hübner K, Nanjee MN, Brinton EA, Mazer NA. An in-silico model of lipoprotein metabolism and kinetics for the evaluation of targets and biomarkers in the reverse cholesterol transport pathway. *PLoS Comput Biol*. 2014;10:e1003509.
13. van de Pas NC, Woutersen RA, van Ommen B, Rietjens IM, de Graaf AA. A physiologically based in silico kinetic model predicting plasma cholesterol concentrations in humans. *J Lipid Res*. 2012;53:2734–2746.
14. Gadkar K, Budha N, Baruch A, Davis JD, Fielder P, Ramanujan S. A mechanistic systems pharmacology model for prediction of LDL cholesterol lowering by PCSK9 antagonism in human dyslipidemic populations. *CPT Pharmacometrics Syst Pharmacol*. 2014;3:1–9.
15. Reyes-Soffer G, Pavlyha M, Ngai C, et al. Effects of PCSK9 inhibition with alirocumab on lipoprotein metabolism in healthy humans. *Circulation*. 2017; 135:352–362.
16. Friedrich CM. A model qualification method for mechanistic physiological QSP models to support model-informed drug development. *CPT Pharmacometrics Syst Pharmacol*. 2016;5:43–53.
17. Lange Y, Ye J, Rigney M, Steck TL. Regulation of endoplasmic reticulum cholesterol by plasma membrane cholesterol. *J Lipid Res*. 1999;40:2264–2270.
18. Lange Y, Ye J, Steck TL. How cholesterol homeostasis is regulated by plasma membrane cholesterol in excess of phospholipids. *Proc Natl Acad Sci U S A*. 2004;101:11664–11667.
19. Bellosta S, Arnaboldi L, Gerosa L, et al. Statins effect on smooth muscle cell proliferation. *Semin Vasc Med*. 2004;4:347–356.
20. Vaughan CJ, Gotto AM. Update on statins: 2003. *Circulation*. 2004;110: 886–892.
21. Pandor A, Ara RM, Tumur I, et al. Ezetimibe monotherapy for cholesterol lowering in 2,722 people: systematic review and meta-analysis of randomized controlled trials. *J Intern Med*. 2009;265:568–580.
22. Mikhailidis DP, Lawson RW, McCormick AL, et al. Comparative efficacy of the addition of ezetimibe to statin vs statin titration in patients with hypercholesterolaemia: systematic review and meta-analysis. *Curr Med Res Opin*. 2011; 27:1191–1210.
23. Chapman MJ. Fibrates in 2003: therapeutic action in atherogenic dyslipidaemia and future perspectives. *Atherosclerosis*. 2003;171:1–13.
24. Steiner G. Fibrates and coronary risk reduction. *Atherosclerosis*. 2005;182: 199–207.
25. Konrad RJ, Troutt JS, Cao G. Effects of currently prescribed LDL-C-lowering drugs on PCSK9 and implications for the next generation of LDL-C-lowering agents. *Lipids Health Dis*. 2011;10:38.
26. Cunningham D, Danley DE, Geoghegan KF, et al. Structural and biophysical studies of PCSK9 and its mutants linked to familial hypercholesterolemia. *Nat Struct Mol Biol*. 2007;14:413–419.
27. Piper DE, Jackson S, Liu Q, et al. The crystal structure of PCSK9: a regulator of plasma LDL-cholesterol. *Structure*. 2007;15:545–552.
28. Giugliano RP, Desai NR, Kohli P, et al. Efficacy, safety, and tolerability of a monoclonal antibody to proprotein convertase subtilisin/kexin type 9 in combination with a statin in patients with hypercholesterolaemia (LAPLACE-TIMI 57): a randomised, placebo-controlled, dose-ranging, phase 2 study. *Lancet*. 2012;380:2007–2017.
29. Millar JS, Reyes-Soffer G, Jumes P, et al. Anacetrapib lowers LDL by increasing ApoB clearance in mildly hypercholesterolemic subjects. *J Clin Invest*. 2015; 125:2510–2522.
30. Okazaki S, Yokoyama T, Miyauchi K, et al. Early statin treatment in patients with acute coronary syndrome: demonstration of the beneficial effect on atherosclerotic lesions by serial volumetric intravascular ultrasound analysis during half a year after coronary event: the ESTABLISH study. *Circulation*. 2004;110: 1061–1068.
31. McQuade ST, Abrams RE, Barrett JS, Piccoli B, Azer K. LIFE methodology: towards a robust mathematical framework for quantitative systems pharmacology simulators. *Gene Regul Syst Biol*. In press.
32. Dodge JT Jr, Brown BG, Bolson EL, Dodge HT. Lumen diameter of normal human coronary arteries. Influence of age, sex, anatomic variation, and left ventricular hypertrophy or dilation. *Circulation*. 1992;86:232–246.
33. Yamagishi M, Terashima M, Awano K, et al. Morphology of vulnerable coronary plaque: insights from follow-up of patients examined by intravascular ultrasound before an acute coronary syndrome. *J Am Coll Cardiol*. 2000;35: 106–111.
34. Sipahi I, Nicholls SJ, Tuzcu EM, Nissen SE. Coronary atherosclerosis can regress with very intensive statin therapy. *Cleve Clin J Med*. 2006;73:937–944.
35. Varnava AM, Mills PG, Davies MJ. Relationship between coronary artery remodeling and plaque vulnerability. *Circulation*. 2002;105:939–943.
36. Hattori K, Ozaki Y, Ismail TF, et al. Impact of statin therapy on plaque characteristics as assessed by serial OCT, grayscale and integrated backscatter-IVUS. *JACC Cardiovasc Imaging*. 2012;5:169–177.
37. van Gils MJ, Vukadinovic D, van Dijk AC, Dippel DW, Niessen WJ, van der Lugt A. Carotid atherosclerotic plaque progression and change in plaque composition over time: a 5-year follow-up study using serial CT angiography. *AJNR Am J Neuroradiol*. 2012;33:1267–1273.
38. Davies MJ, Richardson PD, Woolf N, Katz DR, Mann J. Risk of thrombosis in human atherosclerotic plaques: role of extracellular lipid, macrophage, and smooth muscle cell content. *Br Heart J*. 1993;69:377–381.
39. Kolodgie FD, Narula J, Burke AP, et al. Localization of apoptotic macrophages at the site of plaque rupture in sudden coronary death. *Am J Pathol*. 2000;157:1259–1268.
40. Moreno PR, Falk E, Palacios IF, Newell JB, Fuster V, Fallon JT. Macrophage infiltration in acute coronary syndromes. Implications for plaque rupture. *Circulation*. 1994;90:775–778.
41. Nakata A, Nakagawa Y, Nishida M, et al. CD36, a novel receptor for oxidized low-density lipoproteins, is highly expressed on lipid-laden macrophages in human atherosclerotic aorta. *Arterioscler Thromb Vasc Biol*. 1999;19:1333–1339.

42. Tanaka A, Tearney GJ, Bouma BE. Challenges on the frontier of intracoronary imaging: atherosclerotic plaque macrophage measurement by optical coherence tomography. *J Biomed Opt*. 2010;15:011104.
43. Tearney GJ, Yabushita H, Houser SL, et al. Quantification of macrophage content in atherosclerotic plaques by optical coherence tomography. *Circulation*. 2003;107:113–119.
44. van der Wal AC, Becker AE. Atherosclerotic plaque rupture—pathologic basis of plaque stability and instability. *Cardiovasc Res*. 1999;41:334–344.
45. Virmani R, Kolodgie FD, Burke AP, Farb A, Schwartz SM. Lessons from sudden coronary death: a comprehensive morphological classification scheme for atherosclerotic lesions. *Arterioscler Thromb Vasc Biol*. 2000;20:1262–1275.
46. Bennett MR, Macdonald K, Chan SW, Boyle JJ, Weissberg PL. Cooperative interactions between RB and p53 regulate cell proliferation, cell senescence, and apoptosis in human vascular smooth muscle cells from atherosclerotic plaques. *Circ Res*. 1998;82:704–712.
47. Katsuda S, Coltrera MD, Ross R, Gown AM.. Human atherosclerosis. IV Immunocytochemical analysis of cell activation and proliferation in lesions of young adults. *Am J Pathol*. 1993;142:1787–1793.
48. Lutgens E, de Muinck ED, Kitslaar PJ, Tordoir JH, Wellens HJ, Daemen MJ. Biphasic pattern of cell turnover characterizes the progression from fatty streaks to ruptured human atherosclerotic plaques. *Cardiovasc Res*. 1999;41: 473–479.
49. Robbins CS, Hilgendorf I, Weber GF, et al. Local proliferation dominates lesional macrophage accumulation in atherosclerosis. *Nat Med*. 2013;19: 1166–1172.
50. Cancel LM, Tarbell JM. The role of mitosis in LDL transport through cultured endothelial cell monolayers. *Am J Physiol Heart Circ Physiol*. 2011;300: H769–H776.
51. Cancel LM, Tarbell JM. The role of apoptosis in LDL transport through cultured endothelial cell monolayers. *Atherosclerosis*. 2010;208:335–341.
52. Di Tomaso G, Diaz-Zuccarini V, Pichardo-Almarza C. A multiscale model of atherosclerotic plaque formation at its early stage. *IEEE Trans Biomed Eng*. 2011;58:3460–3463.
53. Karner G, Perktold K. Effect of endothelial injury and increased blood pressure on albumin accumulation in the arterial wall: a numerical study. *J Biomech*. 2000;33:709–715.
54. Sun N, Wood NB, Hughes AD, Thom SA, Xu XY. Fluid-wall modelling of mass transfer in an axisymmetric stenosis: effects of shear-dependent transport properties. *Ann Biomed Eng*. 2006;34:1119–1128.
55. Li BH, Yin YW, Liu Y, et al. TRPV1 activation impedes foam cell formation by inducing autophagy in oxLDL-treated vascular smooth muscle cells. *Cell Death Dis*. 2014;5:e1182.
56. Kawasaki M, Sano K, Okubo M, et al. Volumetric quantitative analysis of tissue characteristics of coronary plaques after statin therapy using three-dimensional integrated backscatter intravascular ultrasound. *J Am Coll Cardiol*. 2005;45: 1946–1953.
57. Tian J, Gu X, Sun Y, et al. Effect of statin therapy on the progression of coronary atherosclerosis. *BMC Cardiovasc Disord*. 2012;12:70.
58. Finn AV, Nakano M, Narula J, Kolodgie FD, Virmani R. Concept of vulnerable/unstable plaque. *Arterioscler Thromb Vasc Biol*. 2010;30:1282–1292.
59. Bentzon JF, Otsuka F, Virmani R, Falk E. Mechanisms of plaque formation and rupture. *Circ Res*. 2014;114:1852–1866.
60. Rader DJ, Alexander ET, Weibel GL, Billheimer J, Rothblat GH. The role of reverse cholesterol transport in animals and humans and relationship to atherosclerosis. *J Lipid Res*. 2009;50:S189–S194.
61. Barter PJ, Caulfield M, Eriksson M. Effects of torcetrapib in patients at high risk for coronary events. *N Engl J Med*. 2007;357:2109–2122.
62. Kühnast S, Fiocco M, van der Hoorn JWA, Princen HMG, Jukema JW. Innovative pharmaceutical interventions in cardiovascular disease: focusing on the contribution of non-HDL-C/LDL-C-lowering versus HDL-C-raising: a systematic review and meta-analysis of relevant preclinical studies and clinical trials. *Eur J Pharma*. 2015;763:48–63.
63. Gaudet D, Kereiakes DJ, McKenney JM, et al. Effect of alirocumab, a monoclonal proprotein convertase subtilisin/kexin 9 antibody, on lipoprotein(a) concentrations (a pooled analysis of 150 mg every two weeks dosing from phase 2 trials). *Am J Cardiol*. 2014;114:711–715.
64. Aird WC. Spatial and temporal dynamics of the endothelium. *J Thromb Haemost*. 2005;3:1392–1406.
65. Azer K. Developing fit-for-purpose physiological models in drug discovery and development—a framework for qualification best practices. *CPT Pharmacometrics Syst Pharmacol*. 2014.
66. Blum CB. Dynamics of apolipoprotein E metabolism in humans. *J Lipid Res*. 1982;23:1308–1316.
67. Brown MS, Goldstein JL. A receptor-mediated pathway for cholesterol homeostasis. *Science*. 1986;232:34–47.
68. Fidge N, Nestel P, Ishikawa T, Reardon M, Billington T. Turnover of apoproteins A-I and A-II of high density lipoprotein and the relationship to other lipoproteins in normal and hyperlipidemic individuals. *Metabolism*. 1980;29: 643–653.
69. Grefhorst A, McNutt MC, Lagace TA, Horton JD. Plasma PCSK9 preferentially reduces liver LDL receptors in mice. *J Lipid Res*. 2008;49:1303–1311.
70. Imamura H, Kawasaki S, Shiga J, Bandai Y, Sanjo K, Idezuki Y. Quantitative evaluation of parenchymal liver cell volume and total hepatocyte number in cirrhotic patients. *Hepatology*. 1991;14:448–453.
71. Istvan ES, Deisenhofer J. Structural mechanism for statin inhibition of HMG-CoA reductase. *Science*. 2001;292:1160–1164.
72. Kovar J, Havel RJ. Sources and properties of triglyceride-rich lipoproteins containing apoB-48 and apoB-100 in postprandial blood plasma of patients with primary combined hyperlipidemia. *J Lipid Res*. 2002;43:1026–1034.
73. Levine TP, Chain BM. Endocytosis by antigen presenting cells: dendritic cells are as endocytically active as other antigen presenting cells. *Proc Natl Acad Sci U S A*. 1992;89:8342–8346.
74. Marbet P, Rahner C, Stieger B, Landmann L. Quantitative microscopy reveals 3D organization and kinetics of endocytosis in rat hepatocytes. *Microsc Res Tech*. 2006;69:693–707.
75. Radhakrishnan A, Goldstein JL, McDonald JG, Brown MS. Switch-like control of SREBP-2 transport triggered by small changes in ER cholesterol: a delicate balance. *Cell Metab*. 2008;8:512–521.
76. Sauro HM, Hucka M, Finney A, et al. Next generation simulation tools: the Systems Biology Workbench and BioSPICE integration. *OMICS*. 2003;7: 355–372.
77. Tavori H, Fan D, Blakemore JL, et al. Serum proprotein convertase subtilisin/kexin type 9 and cell surface low-density lipoprotein receptor: evidence for a reciprocal regulation. *Circulation*. 2013;127:2403–2413.